R Uthirasamy[1], M.Dinesh [2], V. Kumar Chinnaiyan[3] J.Karpagam[4]

J. Electrical Systems 20-2 (2024): 129-141

Regular paper

Advanced Power Converters For Electric Vehicles

Journal of Electrical Systems

Electric Vehicles (EVs) are the sought-out alternative by world countries in declining carbon emissions from the automobiles. The infrastructure for the same is a highly challenging phenomenon, particularly the DC fast EV charging stations provide issues in terms of quick charging time which impacts the overloading and forecasting of the main electric grid. This paper presents the topologies of unidirectional and bidirectional DC to DC converters for EVs. In the proposed system, unidirectional converters are designed for Solar Photovoltaic (SPV) and auxiliary load systems of EVs and the bidirectional converters are designed for main load systems of EVs. To reduce the undulation content in the voltage profile of the proposed DC to DC converter, random pulse width switching technique is implemented. In this article, Re-Lift and Bidirectional converter configurations are designed and simulated using MATLAB/ SIMULINK and the results are validated with the experimental results.

Keywords: Electric Vehicle, Power Converter DC/DC, Solar Photovoltaic

1. Introduction to Electric Vehicle Charging

Fast charging or rapid charging methods are used to recharge the EV batteries with the minimum time period based on the type of charging methods adopted[1]–[4]. In the fast charging technology, within a minimum time period of 20 minutes, an 80 % of the battery packs are get charged. The rapid development of the EV market has led to the enhancement of new infrastructure for charging stations and charging networks. Slow chargers are naturally rated at 3.2 kW, and are mostly used in domestic applications. This type of chargers is not practically suitable for applications such as EV charging and arc-welding, because of high power requirement. Fast chargers are used in car parks and shopping centers, and may charge at rates of 7kW or 22kW for EV applications. A 22kW charger might charge 62kW EV from zero to hundred percent in approximately two and half to three hours. Generally, quick chargers frequently charge using DC charging method; inbuilt rectifiers are used on EV's for AC to DC conversion within the charger rather than relying on the EV's onboard rectifier[5]–[8]. Quick DC chargers are commonly output52kW power, using which common EV battery can be charged in one hour. The general block representation of charging infra is shown in Fig.1 EV cars are designed to charge be charged in both public and homes, however, for more convenience, most EV car owners do the greater part of their charging at home. Even though more charging facilities are available in the residential system, consumers are not satisfied with the provided system

* Corresponding author: [1]Dr.R.Uthirasamy, Professor, Department of Electrical and Electronics Engineering, Mahendra Engineering College, Namakkal India, E-mail: rusamy83@gmail.com
[2]Mr.M.Dinesh, Assistant Professor, Department of Electrical and Electronics Engineering, Mahendra Engineering College, Namakkal India
[3]Dr.V.Kumar Chinnaiyan, Professor, Department of Electrical and Electronics Engineering, Karpagam College of Engineering, Coimbatore
[4]Dr.J.Karpagam, Professor, Department of Electrical and Electronics Engineering, Karpagam Academy of Higher Education, Coimbatore

due to instability in the grid system [9]–[13]. Block diagram representation of triple input single output system for EV is shown in Fig. 2. The equivalent circuit representation of dual output system [14]–[17] is illustrates in Fig. 3.

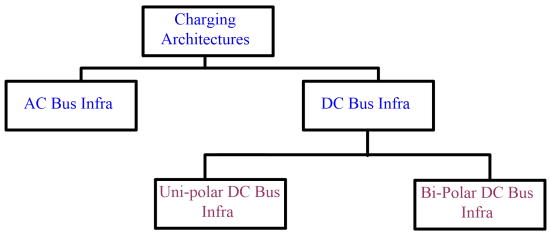

Fig . 1. Block Diagram of Charging Infra.

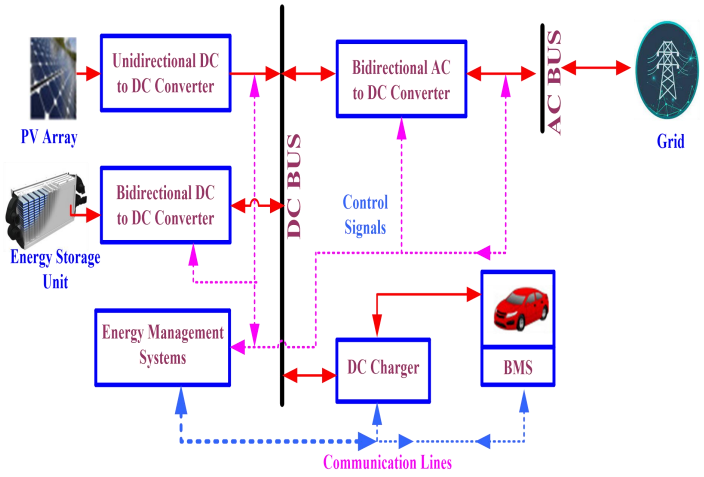

Fig . 2. Triple Input Single Output System for EV Applications

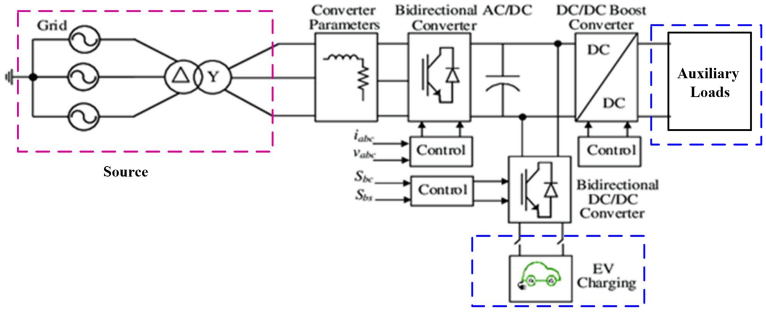

Fig . 3. Dual Output Voltage for EV System

2. DC-DC Converters for EV Shaft Load Systems

Partial power converter is, series-connected with the battery or rectifier unit, where only the difference in voltage between the buses (ΔV) is processed. If the system design is such that the voltage buses are close to each other in value (ΔV small), then the converter processes little power and the losses are minimized. This is in contrast to the full power

processing converter, where P_{loss} is a function of the entire battery bus voltage. With sufficiently low ΔV, P_{loss} decreases and the efficiency increases as a result. If ΔV max is sufficiently small, the converter power rating becomes small. The total power transfer from input to output, however, is not affected. DC Fast charging system for EVs is represented in Fig. 4.

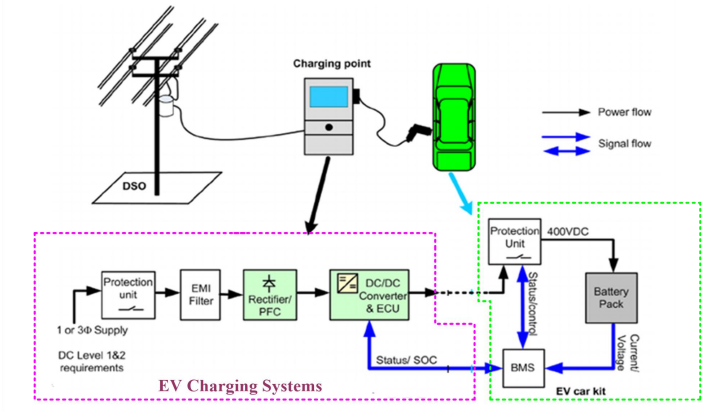

Fig. 4. DC Fast Charging System for EVs

2.1 Bi-directional DC-DC Converter

The proposed converter system is designed to attain both the buck and boost operation for EVs with in-built regenerative braking system. The schematic representation of Bidirectional converter based EV charging is shown in Fig. 5. Whenever the battery is charging, it is activated in buck mode and throughout the discharging it should operate in the boost mode. When the converter consists of low voltage V_L and high voltage V_H sides, the DC bus is connected in the V_H region and battery source is connected in the V_L side of the network. The proposed circuit comprises of two switches named as S_1 and S_2. However, this is trouble-free configuration and is not appropriate for a large choice of applications because the boost voltage gain is incomplete due to the limitations of power semiconductor switches. Thus, the predictable converter is not appropriate for a extensive voltage translation application. The proposed converter has the intrinsic worth of easy configuration and controllability.

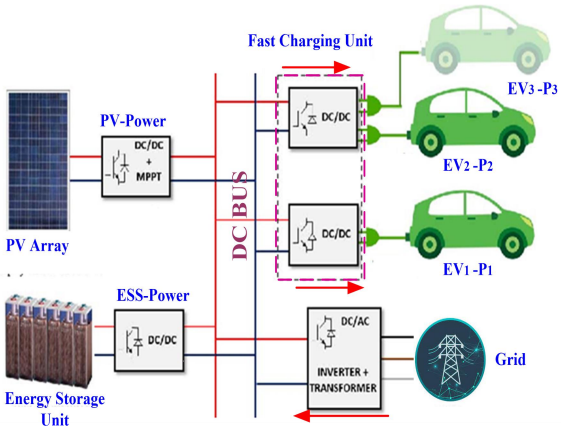

Fig . 5. Bidirectional Converter based EV Charging

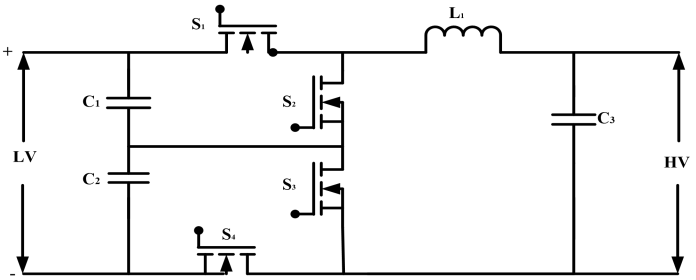

Fig. 6. Circuit Diagram of bi-directional DC to DC converter

The bidirectional converter consists of four number of semiconductor switches named as S_1, S_2, S_3 and S_4 as illustrated in Fig.6. It can be operated in two operating modes; buck-mode and boost-mode, and each mode has three stages of operations. During the buck-mode operation, the high voltage DC bus acts as the source and the battery acts as the load. During the boost-mode operation, the battery acts as the source and the EV acts as the load. The switching states of bi-directional converter operated under buck mode are represented in Table 1. The modes of operation are as follows:

In stage 1, Continuous Conduction Mode (CCM) operation can be obtained in the time period of [t_0-t_1]. In the in-between period, S_3 is designed in such a way to operate as synchronous AC to DC converter. The current all the way through the inductor L_1 is obtained as

$$I_{L1(Step\ Down)} = I_{L1}(t_0) + \left(\frac{1}{L_1}\right) * \left(\left(\frac{V_H}{2}\right) - V_L\right) * (t - t_0) \qquad \text{(Eq 1)}$$

At stage 2, it operates in the time period between [t_1-t_2]. The current through the inductor L_1 is obtained as

$$I_{L1(Step\ Down)} = I_{L1}(t_1) * \left(\frac{V_L}{L_1}\right) * (t_1 - t_2) \qquad \text{(Eq 2)}$$

At stage 3,the converter operates in buck mode, which can be derived between the time interval [t_2-t_3]. Further, the current through the inductor L_1 is obtained as

$$I_{L1(StepDown)} = I_{L1}(t_0) + \left(\frac{1}{L_1} * \left(\left(\frac{V_H}{2}\right) - V_L\right) * (t - t_2)\right) \qquad \text{(Eq 3)}$$

Table 1 Switching States of Bi-directional Converter (Buck Mode)

Stage	ON State Switches	OFF State Switches	Voltage across the Inductor
1	S_1 and S_3	S_2 and S_4	$V_{L1(STEP\ DOWN)} = (V_H / 2)-V_L$
2	S_2 and S_3	S_1 and S_4	$V_{L1\ (STEPDOWN)} = - V_L$
3	S_2 and S_4	S_1 and S_3	$V_{L1\ (STEPDOWN)} = (V_H / 2)- V_L$

2.2. Boost Mode or Step up Mode of Bidirectional DC-DC Converter

Normally, the output voltage from battery is on average 12V, which requires to be boosted to match the load. During this condition, the bi-directional converter is deliberated to function in step-up mode or boost mode. Thus, during the boost mode operation, the battery source behaves as supply for high voltage load. The various operational stages of boost mode are as follows: The stage 1 operation can take place in the time interval of (t_0-

t_1). The energy of the low potential side V_L is transmitted to the inductor L_1. The capacitors S_1 and S_2 are loaded up to discharge for the load RH. The current through the inductor L_1 is obtained as

$$I_{L1(StepUp)} = I_{L1}(t_0) + \left(\left(\frac{V_H}{L_1}\right) * (t - t_0)\right) \qquad \text{(Eq 4)}$$

During stage two operation, step-up mode takes place between the time interval [t_1-t_2]. Thus, the current through the inductor L_1 is given as

$$I_{L1(StepUp)} = I_{L1}(t_1) + \left(\left(\frac{V_L}{L_1}\right) * (t - t_1)\right) \qquad \text{(Eq 5)}$$

The stage 3 operation of step-up mode takes place during the time intervals [t_2– t_3] and the operational principle is the same as the stage one. The I_{L1} is obtained as

$$I_{L1(StepUp)} = I_{L1}(t_2) + \left(\left(\frac{V_L}{L_1}\right) * (t - t_2)\right) \qquad \text{(Eq 6)}$$

Table 2 Switching States of Bi-directional Converter (Boost Mode)

Stage	ON State Switches	OFF State Switches	Voltage across the Inductor
1	S_2 and S_3	S_1 and S_4	V_{L1}(STEPUP) = V_L
2	S_1 and S_3	S_2 and S_4	V_{L1} (STEPUP) = V_L/ (V_H/2)
3	S_1 and S_2	S_3 and S_3	V $_{L1}$ (STEPUP) = V_L

PWM pulses are generated using PIC16F877A microcontroller unit and it is interfaced with driver unit through opto-coupler. In the proposed system three combination of PWM pulses are generated for the MOSFET 16F840 switches S_1, S_2 and S_3. In the microcontroller unit, PWM pulses are generated and analog pulses are taken as output through the port B (Pins 16-18). In the proposed system, IR877 series IC is used to develop the firing pulses with the magnitude of 15 V to the MOSFET switches. PWM Pulses generated for activating the switch 2 and switch 3 are shown in Fig. 7(a). At time T=t_1, the switches S_2 and S_3 are activated, voltage across the inductor is V_{L1} and the output voltage is V_{in} +V_{L1}. At time T=t_2, the switches S_1 and S_3 are activated, in this mode; voltage across the inductor is V_{L1}/ (V_H/2). PWM Pulses generated for activating the switch 1 and switch 3 are shown in Fig. 7 (b). At time T=t_3, the switches S_1 and S_2 are activated, in this mode; voltage across the inductor is V_{in} +V_{L1}.. PWM Pulses generated for activating the switch 1 and switch 2 are shown in Fig. 7 (c).

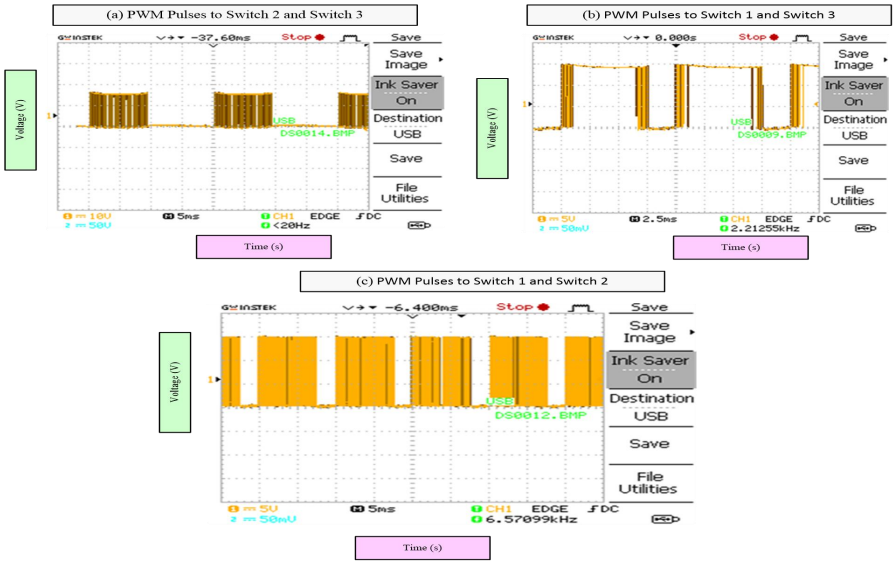

Fig. 7. PWM Firing Pulses to Bidirectional Converter

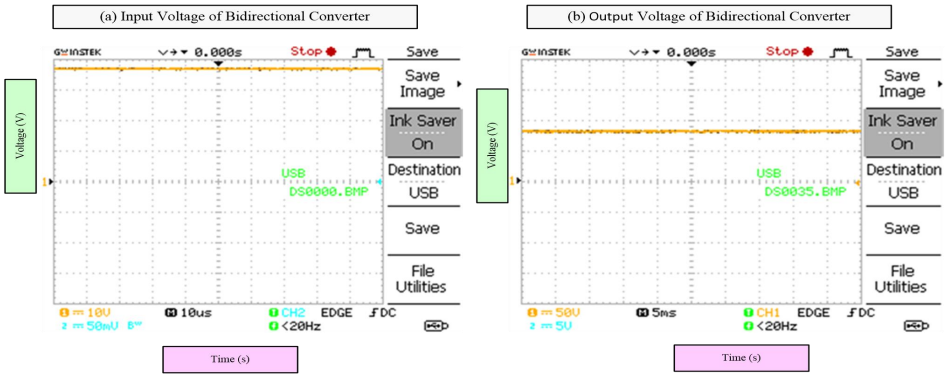

Fig. 8. Input and Output Voltage of Bidirectional Converter

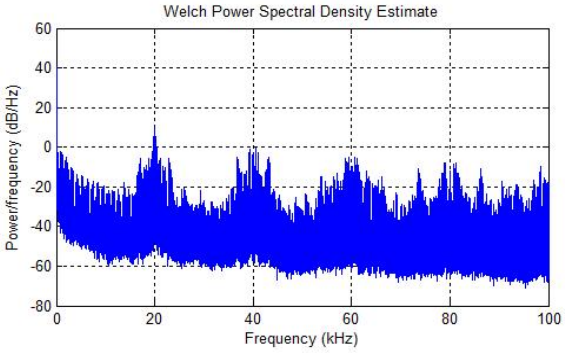

Fig. 9. Power Density Spectrum- Output Voltage

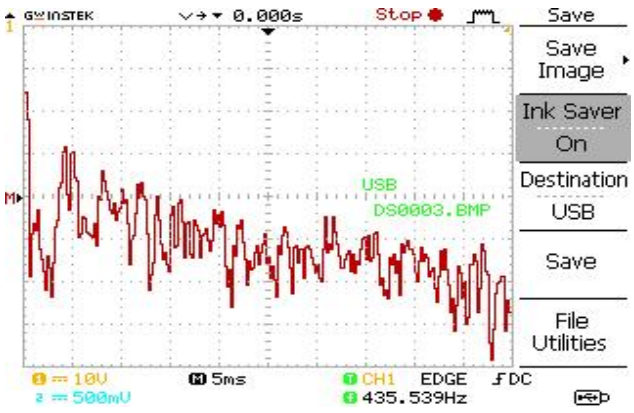

Fig. 10. Output voltage FFT analysis of bidirectional DC to DC converter

Input voltage of bidirectional converter is considered as LV (V_{in}). In the proposed system 38 V is given to the bidirectional DC to DC converter. The bidirectional DC to DC converter acts as a boost converter and the input is boosted to 86 V as shown in the Fig. 8. The power spectral density of the output voltage of the proposed bidirectional DC to DC converter is shown in Fig.9. From the representation it is inferred that the power density spectrum is spread over in the multiples of switching frequency are 11 dB/Hz, 0 dB/Hz, -7 dB/Hz, -11 dB/Hz and -17 dB/Hz for 22 kHz, 42 kHz, 62 kHz, 81 kHz and 100 kHz respectively.

The experimental voltage FFT spectrum of bidirectional DC to DC converter is shown in Fig. 10. From the spectrum it is represented that the bidirectional DC to DC converter system has abridged voltage stress in the multiples of switching frequency (voltage values are negative). The experimental setup of the proposed bidirectional DC to Dc converter is

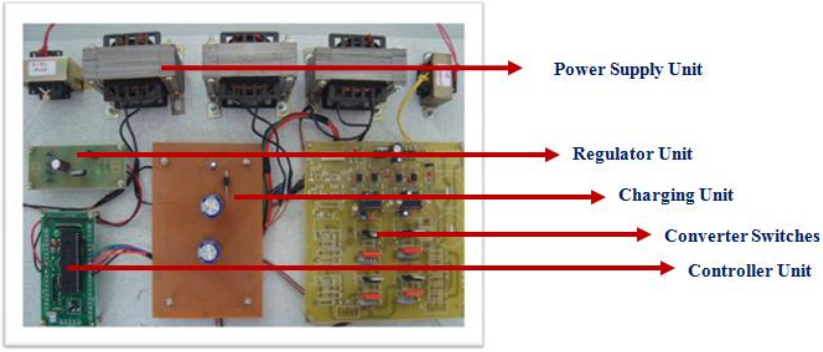

Fig. 11. Experimental setup of bidirectional DC to DC converter

3. Single Input Dual Output (SIDO) chopper

Single Input Dual Output (SIDO) configuration is the cascade connection of Single-Ended Primary-Inductor Converter (SEPIC) and boost chopper configuration. SEPIC and boost operation is achieved through the single switch arrangement. The block diagram representation of SIDO converter configuration is shown in Fig. 12.

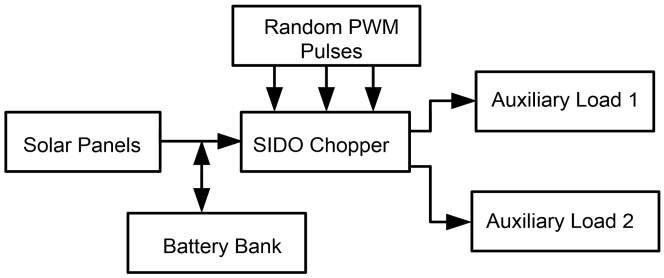

Fig. 5. Block Diagram of solar fed SIDO chopper

3.1 Random Pulse Width Modulation

RPWM is predictably adopted to regulate and minimize the ripple content present in the output voltage. In PWM switching technique as represented in Fig. 13,c the duty cycle is varied randomly based on the desired output voltage. During steady-state operation, the duty ratio of the transition is maintained as constant. Fixed and constant duty cycle is not suited for all conditions of EV application. Thus, based on the load profile of EV, the output power has to be varied dynamically. The random switching technique is adopted for the proposed SEPIC/Boost converter to maintain constant ripple free output voltage. In the RPWM technique, carrier frequency is fixed for generating random switching. In conventional PWM technique the delay to the start of each cycle (εD) is zero and the other parameters such as switching period (TD), on-time (αD) and the duty cycle (D) are kept constant.

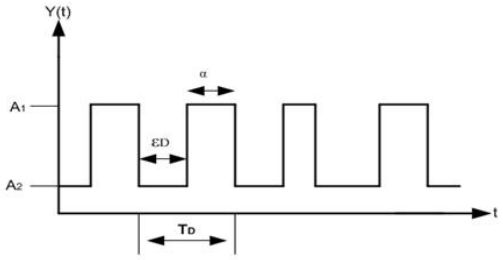

Fig.13. 6RPWM switching pulses

In RPWM, the width of the triggering pulse varies in each switching cycle; αD is randomized and hence the duty cycle is randomized (dD= αD/ TD). The other parameter such as εD is zero and TD is kept constant. This technique is used is to vary the period of the triangular carrier wave randomly. The carrier wave must have linearity and it must have straight line segments. It is alleged with the intention of the immediate transporter occurrence f_{cr} is always larger than command frequency f_{co}. The instantaneous value of carrier frequency can be given as

$$f_c = \frac{1}{(t_d+(1-t_d))} = f_{c0} + \Delta f_c \qquad \text{(Eq 7)}$$

where the change in the frequency is given by

$$\Delta f_c = \left(f_{c,max} - f_{c0}\right) * n(t) \qquad \text{(Eq 8)}$$

3.2 SIDO Chopper

The proposed topology gives two output voltage levels of different magnitude and same polarity. The positive boosted output voltage is obtained from boost chopper and positive

output buck/boost output voltage is attained from SEPIC converter. The equivalent structure of SIDO chopper is shown in Fig. 13& Fig. 14.

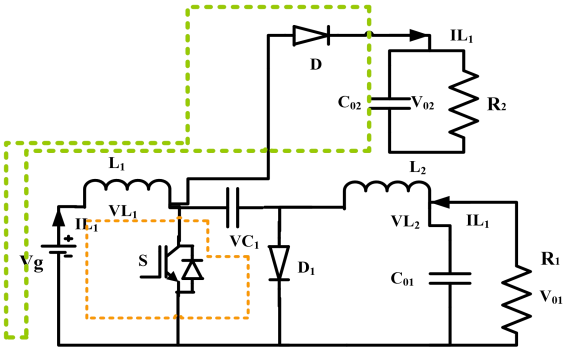

Fig. 74. Equivalent circuit of SIDO chopper- Boost Mode

Mode I: When S is ON

When S is triggered with firing pulses generated using Random Pulse Width Modulation Technique (RPWM) techniques, inductor L_1 is charged by the input voltage and inductor L_2 is by capacitor C_1. The output voltage is maintained by the capacitors available across the load. The energy accumulated in the capacitor is pardoned all the way through the particular loads.

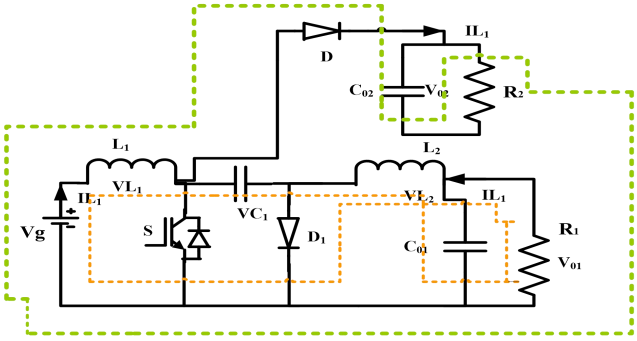

Fig. 85. Equivalent circuit of SIDO chopper – Buck/Boost Mode

Mode II When S is OFF

When the power semiconductor S is in open circuit, the diode D is forward biased. Along with the input voltage and current through inductor L_1, Capacitor C is charged, which feeds the load. In SEPIC configuration the diode gets switched ON, and the inductor current charges the capacitor and performs the load operation. The output voltage from the SEPIC converter is diverse by shifting the duty cycle of the switch.

3.3 Results and Discussion of SIDO Converter Systems

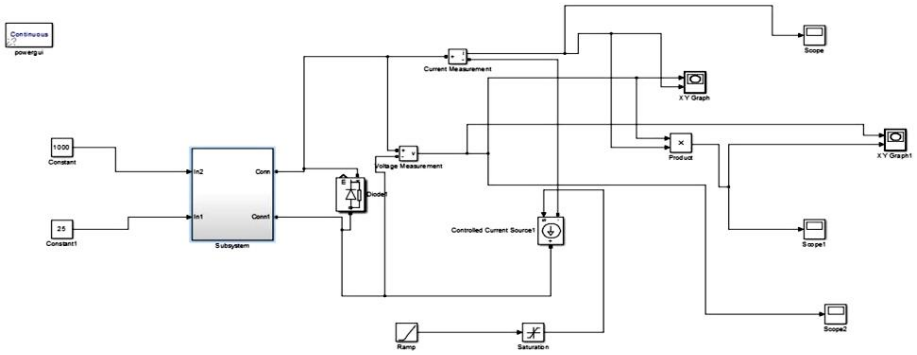

Fig. 9. Simulation Model of SIDO converter

The simulation is carried out as shown in Fig.16 and analyzed by means of MATLAB for the input and the voltage profile of DC output voltage of 38 V (V_{max}) and 110 V (V_{max}) respectively. The system is experimented for the same input and output voltage and the results are validated. Random PWM technique is adopted for triggering pulse generation and the SIDO system is simulated using SIMULINK tool, the PWM pulses as shown in Fig. 17 (a). The entire system simulated for the output voltage of 110 V with an input of 38 V. The performance of the simulated SIDO system are shown in Fig. 17 (b) and 17 (c) respectively. The power density for the inverter voltage of the proposed converter at 10 kHz, 20 kHz, 30 kHz and 40 kHz are -2 dB/Hz, 14 dB/Hz, -16 dB/Hz and 4 dB/Hz respectively as shown on Fig. 17 (d).

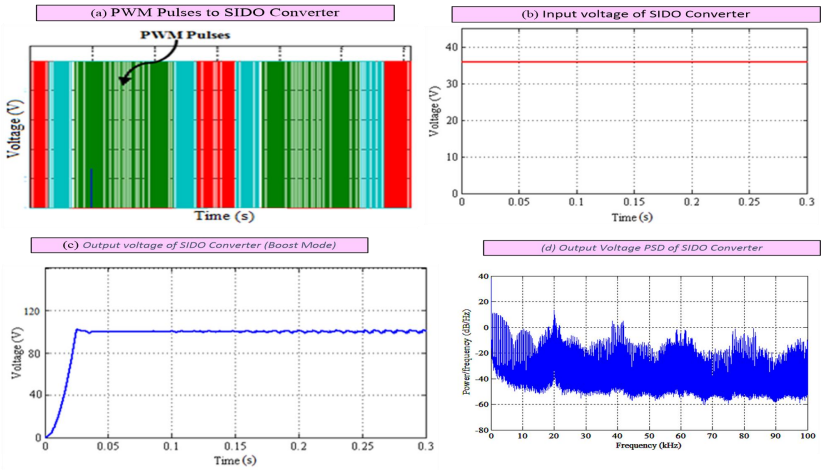

Fig. 10. Simulated results of SIDO Converter

To validate the performance of SIDO converter system, Random PWM pluses are developed using PIC 16F877 controller and the PWM pulses are boosted using driver IC as shown inFig. 18. MOSFT 16F840 switch is triggered using the random PWM pulses, which is used to step-up the input voltage of 38 V to 110 V as shown in Fig. 19. In order to highlight the performance of the SIDO system, a comparative analysis has been made and represented in the Table 3.

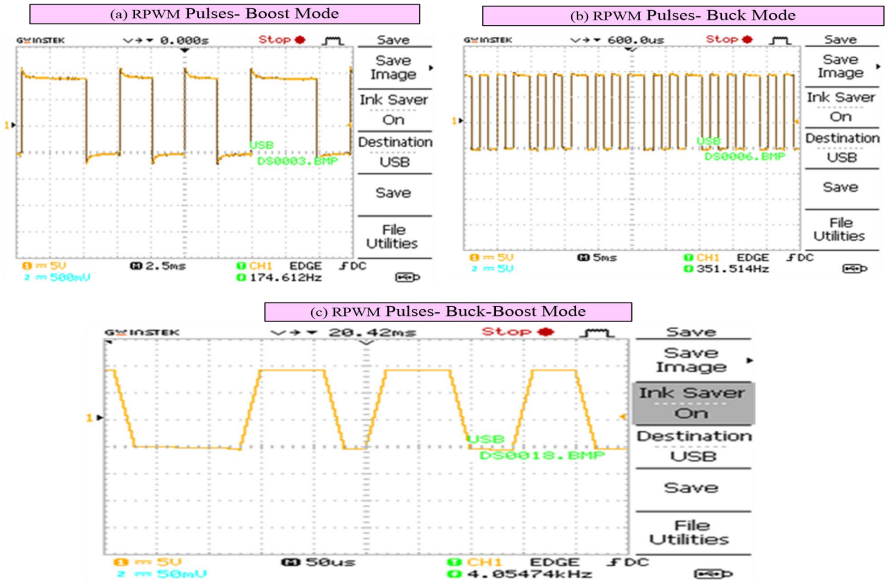

Fig. 18. Random PWM Pulses to Switch (S)

The comparative analysis of various DC to DC converters is represented in the above table. From the analysis, it is inferred that each and every converters have it's own merits and demerits. Based on application of the particular converter, the merits of the each has been highlighted. Voltage stress is zero in SAZZ converter, but on the other side bidirectional property has been restricted. Likewise, Re-Lift converters are perfectly designed for EV fast charging and the bidirectional converter is designed and implemented for EV applications. The experimental setup of the proposed SIDO system is shown in Fig. 20.

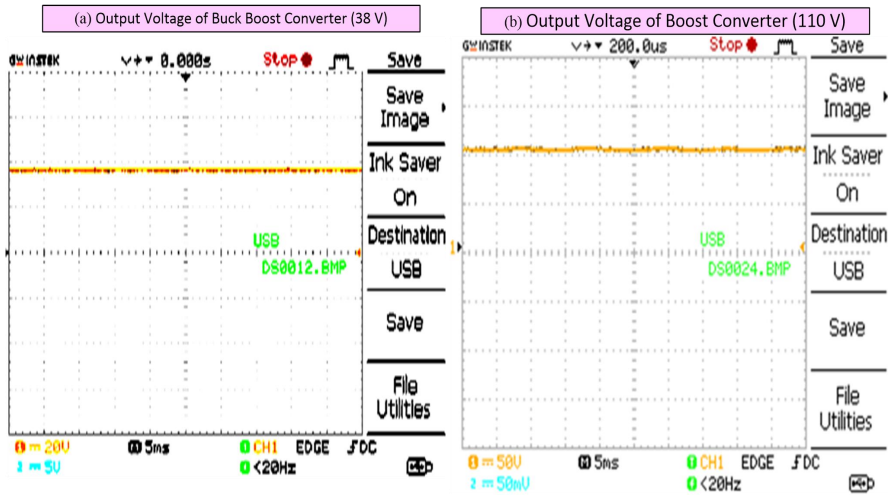

Fig.19. Input and Output Voltage of Boost Converter

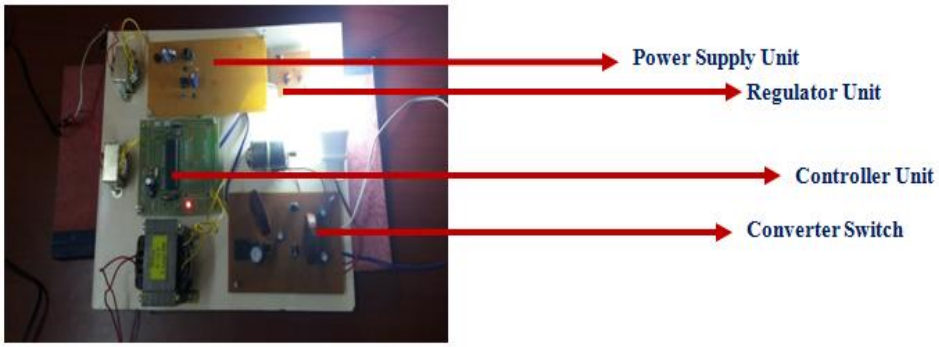

Fig. 20. Experimental Setup of the Proposed SIDO converter system

4. CONCLUSION

In this Chapter, several conventional and advanced DC-DC converters have been reviewed, discussed and further inferences have been provided for different converters in EV battery charging operation. An advanced and promising bidirectional DC-DC converters such as Snubber Assist Zero-Voltage Zero-Current (SAZZ) converter and Re-Lift Converter have been introduced along with their topologies and control strategies have been discussed for EV fast-charging operation which flows power in a bidirectional way in between Vehicle to Grid and Grid to Vehicle should be such that it has reduced the impacts in Power Grid in terms of load levelling, peak load shaving and improve voltage regulation and stability of power grid station.

REFERENCES

[1] S. Hemavathi, "Modeling and energy optimization of hybrid energy storage system," Hybrid Renewable Energy Systems, pp. 97–114, 2021.

[2] S. Hemavathi, "Modeling of analog battery management system for single cell lithium ion battery," Energy Storage, pp. 1–9, 2020.

[3] S. Hemavathi, "Overview of cell balancing methods for Li-ion battery technology," Energy storage, vol. 203, pp. 1–12, 2020.

[4] S. Hemavathi, "Li-ion battery health estimation based on battery internal impedance measurement," in Innovations in Sustainable Energy and Technology, Springer, 2021, pp. 183–193.

[5] M. S. Agamyet al., "A high power density DC-DC converter for distributed PV architectures," IEEE Conference on Photovoltaic Specialists, pp. 1–8, Oct. 2014, doi: 10.1109/PVSC-VOL2.2012.6656721.

[6] S. Hemavathi, "Modeling and Estimation of Lithium-ion Battery State of Charge Using Intelligent Techniques," in Advances in Power and Control Engineering, Springer, 2020, pp. 157–172.

[7] S. Hemavathi and M. Singh, "Microgrid Short Circuit Studies," 8th IEEE Power India International Conference, PIICON 2018, Jul. 2018, doi: 10.1109/POWERI.2018.8704389.

[8] D. M. Bellur and M. K. Kazimierczuk, "DC-DC converters for electric vehicle applications," 2007 Electrical Insulation Conference and Electrical Manufacturing

Expo, EEIC 2007, pp. 286–293, 2007, doi: 10.1109/EEIC.2007.4562633.

[9] G. Chen, Y. S. Lee, S. Y. R. Hui, D. Xu, and Y. Wang, "Actively clamped bidirectional flyback converter," IEEE Transactions on Industrial Electronics, vol. 47, no. 4, pp. 770–779, Aug. 2000, doi: 10.1109/41.857957.

[10] L. Chen, H. Wu, P. Xu, H. Hu, and C. Wan, "A high step-down non-isolated bus converter with partial power conversion based on synchronous LLC resonant converter," Conference Proceedings - IEEE Applied Power Electronics Conference and Exposition - APEC, vol. 2015-May, no. May, pp. 1950–1955, May 2015, doi: 10.1109/APEC.2015.7104614.

[11] R. Y. Duan and J. D. Lee, "High-efficiency bidirectional DC-DC converter with coupled inductor," IET Power Electronics, vol. 5, no. 1, pp. 115–123, Jan. 2012, doi: 10.1049/IET-PEL.2010.0401.

[12] M. M. Ghahderijani, M. Castilla, A. Momeneh, J. T. Miret, and L. G. de Vicuna, "Frequency-Modulation Control of a DC/DC Current-Source Parallel-Resonant Converter," IEEE Transactions on Industrial Electronics, vol. 64, no. 7, pp. 5392–5402, Jul. 2017, doi: 10.1109/TIE.2017.2677321.

[13] J. W. Kimball and P. T. Krein, "Singular Perturbation Theory for DC—DC Converters and Application to PFC Converters," IEEE Trans Power Electron, vol. 23, no. 6, pp. 2970–2981, 2008, doi: 10.1109/TPEL.2008.2004272.

[14] T. Konjedic, L. Korošec, M. Truntič, C. Restrepo, M. Rodič, and M. Milanovič, "DCM-based zero-voltage switching control of a bidirectional DC-DC converter with variable switching frequency," IEEE Trans Power Electron, vol. 31, no. 4, pp. 3273–3288, Apr. 2016, doi: 10.1109/TPEL.2015.2449322.

[15] A. Morrison, J. W. Zapata, S. Kouro, M. A. Perez, T. A. Meynard, and H. Renaudineau, "Partial power DC-DC converter for photovoltaic two-stage string inverters," ECCE 2016 - IEEE Energy Conversion Congress and Exposition, Proceedings, 2016, doi: 10.1109/ECCE.2016.7855332.

[16] M. Kwon, S. Oh, and S. Choi, "High gain soft-switching bidirectional DC-DC converter for eco-friendly vehicles," IEEE Trans Power Electron, vol. 29, no. 4, pp. 1659–1666, 2014, doi: 10.1109/TPEL.2013.2271328.

[17] Hemavathi S and K Nithiyananthan, "DC to DC Energy Conversion using Novel loaded Resonant Converter," International Journal of Power Control and Computation, vol. 7, no. 2, pp. 113–122, 2015.